

Amplitude analysis of the $K_S^0 K_S^0$ system produced
in the reaction $\pi^- p \rightarrow K_S^0 K_S^0 n$ at 23 GeV/c

A. Etkin, K. J. Foley, R. S. Longacre, W. A. Love, T. W. Morris, S. Ozaki,* E. D. Platner,
V. A. Polychronakos, A. C. Saulys, Y. Teramoto,† C. D. Wheeler, and E. H. Willen
Brookhaven National Laboratory, Upton, New York 11973

K.-W. Lai

*Brookhaven National Laboratory, Upton, New York 11973
and University of Arizona, Tucson, Arizona 85721*

S. J. Lindenbaum

*Brookhaven National Laboratory, Upton, New York 11973
and City College of New York, New York, New York 10031*

M. A. Kramer and U. Mallik‡

City College of New York, New York, New York 10031

W. A. Mann and R. Merenyi

Tufts University, Medford, Massachusetts 02155

J. Marraffino, C. E. Roos, and M. S. Webster

Vanderbilt University, Nashville, Tennessee 37235

(Received 28 August 1981; revised manuscript received 6 November 1981)

We have carried out an amplitude analysis of the $K_S^0 K_S^0$ system produced in the reaction $\pi^- p \rightarrow K_S^0 K_S^0 n$ at 23 GeV/c, based on about 15 000 events in the low- t region ($|t - t_{\min}| < 0.1 \text{ GeV}^2$). Below 1.6 GeV/c², our favored solution is very similar to those from previous analyses. For higher masses, we observe the $K_S^0 K_S^0$ decay of the $h(2040)$ meson. In addition, the $l=0$ partial wave contains a new state, strongly coupled to $K_S^0 K_S^0$, with parameters $M = 1.771_{-0.053}^{+0.077} \text{ GeV}/c^2$ and $\Gamma = 0.200_{-0.009}^{+0.156} \text{ GeV}/c^2$. Since this state is most probably $I=0$, we call it the $S^*(1770)$. We find an f'/f production ratio of $0.23_{-0.13}^{+0.14}$, and branching ratios for f -meson and $h(2040)$ -meson decays into $K\bar{K}$ of $(3.1_{-1.7}^{+0.7})\%$ and $(0.67_{-0.15}^{+0.41})\%$, respectively. We find, in a detailed comparison of our results with those from other experiments, that our solution is compatible with all known features of both charged and neutral $K\bar{K}$ systems.

I. INTRODUCTION

We present the analysis of an experiment performed at Brookhaven National Laboratory using the Multiparticle Spectrometer (MPS) facility to study the reaction

$$\pi^- p \rightarrow K_S^0 K_S^0 n$$

at 23 GeV/c. Several features of the $K_S^0 K_S^0$ system, and more generally, the $K\bar{K}$ system, have attracted considerable interest. The $K_S^0 K_S^0$ effective-mass spectrum has been known to contain a very rich structure since the earliest low-statistics experi-

ments. In addition, the indistinguishability of the two K_S^0 's restricts the set of quantum states the $K_S^0 K_S^0$ system may populate to $C = +1$, $J^P = (\text{even})^+$, and $I^G = 0^+$ or 1^- . The fact that the ground state of the glueball spectrum should occur in the $J^{PC} = 0^{++}$ and 2^{++} is also worthy of note. In fact, the presence of glueball or $2q2\bar{q}$ states may help explain why our understanding of the $K_S^0 K_S^0$ system is still incomplete and somewhat confused, particularly with regard to the scalar mesons. The recent literature¹⁻⁷ on the subject demonstrates this point. Experiments involving $K\bar{K}$ final states other than $K_S^0 K_S^0$ (Refs. 8-14) likewise agree in

general, but differ in detail. In short, the present status of meson spectroscopy in $K\bar{K}$ final states can be described as unclear.

Beyond that, it is also true that previous $K_S^0 K_S^0$ analyses have been somewhat limited by a lack of statistics. In that context, we note that our data sample contains three to four times as many events as that from any previous experiment. To our knowledge, this is the first experiment to have sufficient sensitivity at relatively high effective mass to observe the $K_S^0 K_S^0$ decay mode of the $h(2040)$ meson.

In Sec. II, we describe the experimental method and the reduction of the raw data. Our moments and amplitude analyses are discussed in Secs. III and IV, respectively. We describe our results and compare them with those from previous analyses in Secs. V and VI. Section VII summarizes our results and conclusions.

II. EXPERIMENTAL METHOD AND DATA REDUCTION

This experiment was performed in the Brookhaven National Laboratory Multiparticle Spectrometer (MPS) using a 23.0-GeV/c unseparated negative beam incident on a 61-cm-long liquid hydrogen target. A small flux of K^- 's and \bar{p} 's was identified by means of two threshold Čerenkov counters. The target was positioned in the 10-kG magnetic field of the MPS and surrounded by an array of anticoincidence counters as shown in Fig. 1. Downstream of the target, there was an array

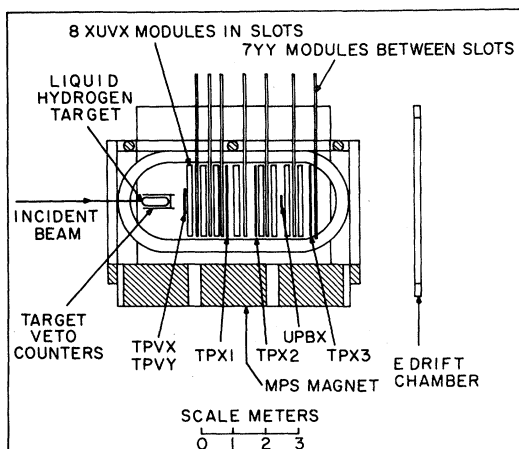


FIG. 1. The configuration of the MPS for this experiment.

of 46 magnetostrictive-spark-chamber planes with X (horizontal), Y (vertical), U , and V readouts (where U and V are $+15^\circ$ and -15° from the Y axis, respectively), and six planar proportional wire chambers indicated in Fig. 1. In addition, a three-plane, large-aperture, X -measuring drift chamber, positioned approximately 6 m downstream of the target, was used to improve the momentum resolution of fast forward tracks. More detailed descriptions of the MPS can be found in Refs. 15 and 16.

The trigger was designed to select interactions with initially neutral final states where at least two particles decayed into charged particles. These requirements were met by demanding no signal from a veto-counter system around the target and three or more hits in either of the proportional wire chambers identified as $TPX1$ and $TPX2$ in Fig. 1. The efficiency of the downstream veto counter was measured to be at least 99.99%. The top, bottom, and side elements of the target anticoincidence-counter system were scintillator-lead shower counters, and thus also discriminated against recoil systems involving π^0 's. We recorded 2.1×10^6 triggers at a rate of ~ 1 trigger per 75×10^3 beam π^+ 's.

These triggers were analyzed by a computer program which recognized and then fitted tracks individually. For events with at least four such tracks, the program searched for all combinations of two oppositely charged tracks which formed a vertex downstream of the target veto counters and upstream of $TPX2$. For those events where at least two such combinations were found, each combination was tested for kinematical consistency with K^0 , Λ , or $\bar{\Lambda}$ decay. A neutral vee was accepted as a K^0 decay if the effective mass for the $\pi^+\pi^-$ hypothesis was between 0.475 and 0.525 GeV/c^2 . In a few cases, more than two combinations remained due to ambiguities in pairing the tracks. For those events, the two combinations with the smallest deviations from the nominal K^0 mass were retained. The lines of flight of the K^0 's were then extrapolated upstream to determine the position of the production vertex. The requirement was imposed that the two extrapolated tracks pass within 1 cm of each other. For those events with $K_S^0 K_S^0$ effective mass below $\sim 1.1 \text{ GeV}/c^2$, the error on the interaction point generally had a large component along the beam direction. Hence no target cut was used on the final data sample. A series of target-empty runs was taken in addition to the target-full runs. Analysis of the target-empty data showed that these events had distribu-

tions similar to those from target-full runs. Therefore we have applied a uniform cross-section correction of 6% to the total data sample. The K^0 mass spectrum is shown in Fig. 2(a) and the (missing mass)² (MM^2) spectrum for all events with two accepted K^0 decays is shown in Fig. 2(b). The resolution is 0.004 GeV/ c^2 (rms) for the K^0 mass, and 0.3 (GeV/ c^2)² (rms) for (missing mass)², consistent with Monte Carlo predictions.

Neutron-recoil events were selected by requiring that MM^2 be less than 1.4 (GeV/ c^2)². With this cut we estimate $\sim 7\%$ contamination of N^* in the "neutron" sample. The final data sample contained 29 381 $\pi^- p \rightarrow K_S^0 K_S^0 n$ events. After the above mentioned cuts, the final data sample contained a negligible contamination from the reaction $\pi^- p \rightarrow K^0 \Lambda + X^0$. This was determined by reconstructing the accepted K^0 events using Λ or $\bar{\Lambda}$ decay kinematics. No Λ or $\bar{\Lambda}$ signal above background was observed.

Figure 3 shows the $K_S^0 K_S^0$ invariant-mass spectrum for the entire data sample and for the 15 359 events with $t' < 0.1$ (GeV/ c)², where $t' = |t - t_{\min}|$,

$$d^4\sigma/dt'dM d\Omega = N(M, t') I(\Omega) = N(M, t') \sum_l [\langle Y_l^0 \rangle Y_l^0(\Omega) + 2 \sum_m \langle Y_l^m \rangle \text{Re} Y_l^m(\Omega)],$$

where $\Omega = (\cos\theta, \phi)$ gives the direction of one of the K_S^0 s in the Gottfried-Jackson frame and M is the $K_S^0 K_S^0$ invariant mass. $N(M, t')$ is proportional to $d^2\sigma/dt'dM$ and gives the number of events observed in a given t' and M bin. The expansion

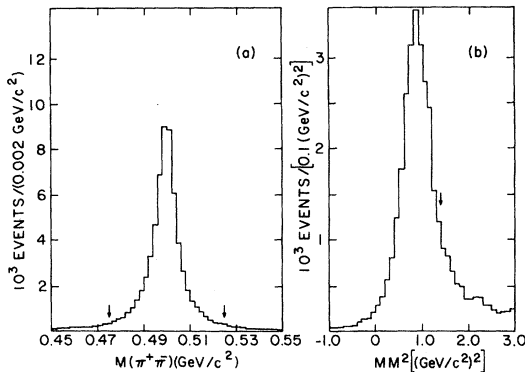


FIG. 2. (a) The $\pi^+ \pi^-$ effective-mass spectrum with all cuts used in the analysis. The arrows indicate the mass range of events selected as K_S^0 . (b) The missing-mass-squared spectrum of all $K_S^0 K_S^0$ events with all cuts used in the analysis. The arrow indicates the mass range for neutron-recoil selection.

and t is the square of the four-momentum transfer from the beam to the outgoing $K_S^0 K_S^0$ system. Using the acceptance-corrected cross section in the low- t region and correcting for neutral K_S^0 decays, we obtain an average sensitivity of ~ 15 events/nb. The general characteristics of the mass spectrum are the previously observed peaks at threshold and in the $f_2 A_2$ region, along with some evidence of new structure at higher mass.

We shall, for the most part, restrict our attention to the $t' < 0.1$ (GeV/ c)² data in order to isolate the pion-exchange contribution to the $K_S^0 K_S^0$ production amplitudes. As shown in Ref. 10, one-pion-exchange processes dominate all others by a factor of ~ 40 in this t' range. Furthermore, one-pion exchange selects the $I^G = 0^+$ state.

III. MOMENTS ANALYSIS

We have expanded our experimental angular distribution in terms of normalized spherical harmonics:

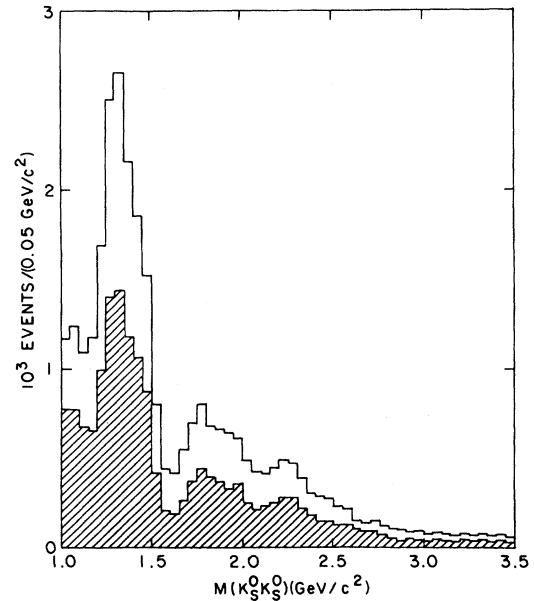


FIG. 3. The $K_S^0 K_S^0$ effective-mass spectrum with all cuts for analysis. The singly hatched part of the histogram contains all events with $0.0 < t' < 0.1$ (GeV/ c)².

coefficients $\langle Y_l^m \rangle$ are the moments of the spherical harmonics. If the acceptance of the spectrometer were uniform in Ω , these moments would be given simply by

$$\langle Y_l^m \rangle = \int \text{Re} Y_l^m(\Omega) I(\Omega) d\Omega / \int I(\Omega) d\Omega .$$

Since the MPS acceptance is not uniform, we have performed a Monte Carlo simulation of the spectrometer acceptance. We have generated Monte Carlo events uniformly in $\cos\theta$ and ϕ modified by a factor $e^{bt'}$, where $b = -8.0 \text{ (GeV/c)}^{-2}$ was chosen to approximately match the experimental t' distribution. The results obtained were insensitive to reasonable variations of this parameter. A set of such events was generated at 0.1-GeV/ c^2 steps in $K_S^0 K_S^0$ effective mass from threshold up to 1.6 GeV/ c^2 and at 0.2-GeV/ c^2 steps from 1.6 GeV/ c^2 up to 3.0 GeV/ c^2 . These events were generated at the level of raw coordinates in the various detectors so that all known distortions, inefficiencies and background effects could be simulated realistically. In this form, the Monte Carlo events were analyzed by the same programs used for the data with all of the same cuts and selection criteria. We stress that this method accounts not only for geometric acceptance, but many other systematic biases as well. This includes, for instance, the effects of cuts on the data, counter and spark-chamber efficiencies, and the efficiency of the track-finding program. The reconstructed Monte Carlo events thus represent a measure of the absolute acceptance for the data under conditions where $N(M, t')$ and $I(\Omega)$ are known. For those events, we define $A(M, t', \Omega) = N(M, t') I(\Omega)$ and expand it in terms of spherical harmonics, denoting the expansion coefficients by G_l^m . Note that the G_l^m are functions of M and t' . The mass dependence of the G_l^m was approximated by a cubic spline fit to the discrete values obtained from the Monte Carlo events. The acceptance-corrected data moments, $\langle Y_l^m \rangle$, are then those values which minimize the negative of the extended logarithmic likelihood function

$$\mathcal{L} = \sum_i \ln I(\Omega_i) - \sum_{lm} G_l^m \langle Y_l^m \rangle .$$

The first sum (i) is over events for a set of mass bins described below; the corresponding G_l^m were evaluated at the bin centers using the spline fit coefficients. The second sum runs over all even $l \leq 8$ and all $m \leq 2$. The program MINUIT (Ref. 17) was used to minimize this function. The $K_S^0 K_S^0$ effective mass was divided into 0.025-GeV/ c^2 inter-

vals for $M(K_S^0 K_S^0) < 1.6 \text{ GeV}/c^2$, then into 0.05-GeV/ c^2 intervals up to $M(K_S^0 K_S^0) = 2.0 \text{ GeV}/c^2$, and finally into 0.1-GeV/ c^2 intervals up to $M(K_S^0 K_S^0) = 2.5 \text{ GeV}/c^2$. These intervals were chosen to give a reasonable number of events in each bin. Even though we had events with larger mass values, we terminated the moments calculation at $M(K_S^0 K_S^0) = 2.5 \text{ GeV}/c^2$ because our acceptance vanished for some values of $\cos\theta$ and ϕ beyond that mass, making it difficult to calculate the higher moments. Our mass resolution, ranging from 0.004 GeV/ c^2 (rms) at 1.2 GeV/ c^2 to 0.021 GeV/ c^2 (rms) at 2.4 GeV/ c^2 , was always less than the bin size.

All $m=2$ moments, together with $\langle Y_6^1 \rangle$ and $\langle Y_8^1 \rangle$, were found to be consistent with zero in this t' range. The remaining seven significant moments are shown in Fig. 4. The smooth curves in Fig. 4 will be discussed in Sec. IV. As a check of our procedure, we have repeated the entire calculation expanding in terms of the imaginary part of the $Y_l^m(\Omega)$ and found all moments to be consistent with zero as required by parity conservation.

It is possible to draw some qualitative, but nonetheless significant, conclusions from the moments alone before proceeding to a discussion of the underlying amplitudes. First, we note that the plot of $\langle Y_0^0 \rangle$ in Fig. 4 is the acceptance-corrected $K_S^0 K_S^0$ effective-mass spectrum. Second, the absence of any significant $m=2$ moments, together with the relatively small $m=1$ moments, implies that the production of $K_S^0 K_S^0$ systems is dominated by states of zero helicity in the t channel. Third, the presence of large negative excursions in the $\langle Y_2^0 \rangle$ moment, notably at $M(K_S^0 K_S^0) = 1.2 \text{ GeV}/c^2$ and again at $M(K_S^0 K_S^0) = 1.8 \text{ GeV}/c^2$, indicate rather strong interference between either S and D waves or D and G waves. The presence of so much interference seems, to us, to preclude drawing any detailed conclusions from the $K_S^0 K_S^0$ effective-mass spectrum alone. Moreover, the $\langle Y_4^0 \rangle$ moment shows a rather broad structure around 1.3 GeV/ c^2 which cannot be attributed solely to f -meson production. Finally, the $\langle Y_6^0 \rangle$ and $\langle Y_8^0 \rangle$ moments show clear evidence of G -wave structure near $M(K_S^0 K_S^0) = 2.0 \text{ GeV}/c^2$, which we associate with the $h(2040)$ meson.

IV. AMPLITUDE ANALYSIS

The experimental moments are related to the production amplitudes through a set of coupled

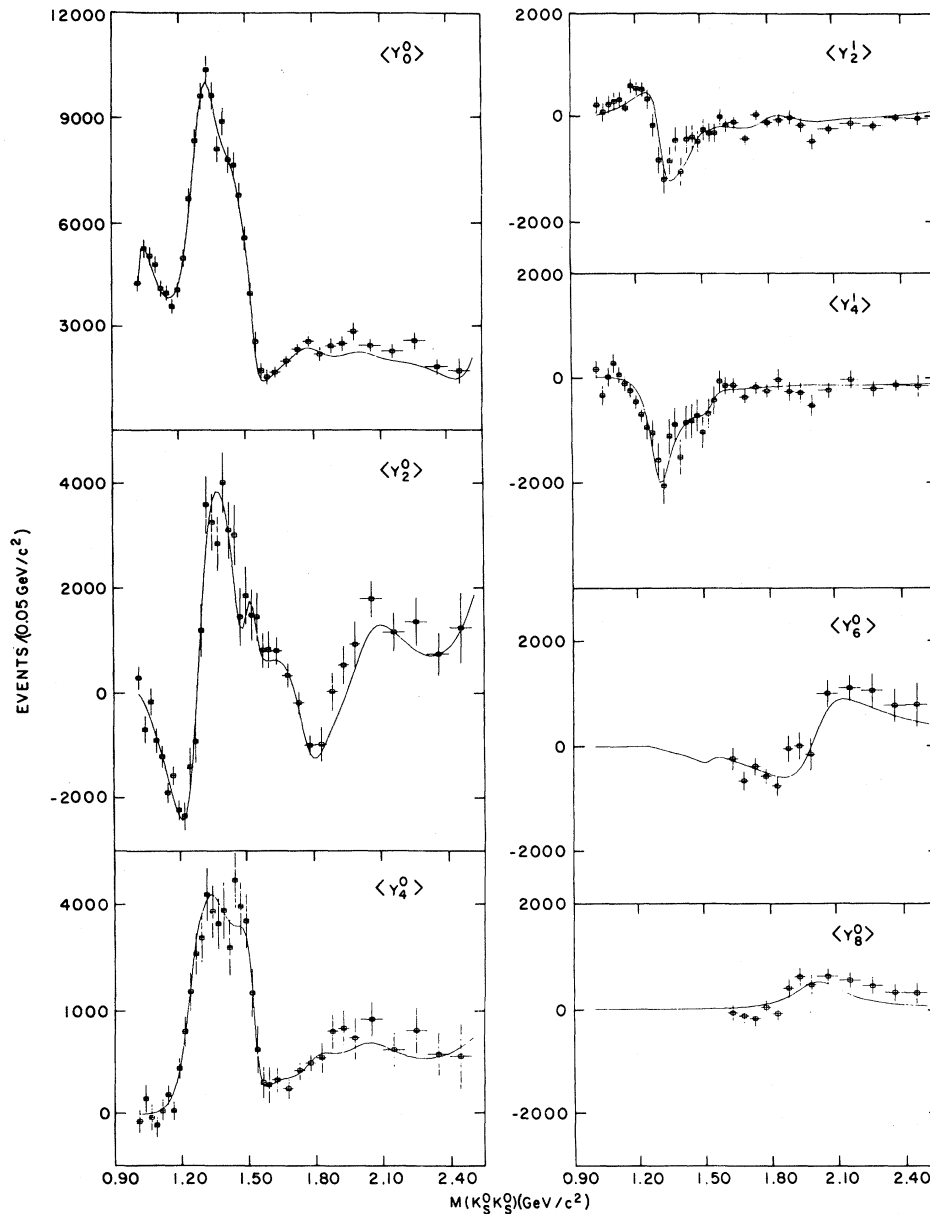


FIG. 4. The acceptance-corrected, unnormalized t -channel moments $\langle Y_l^m \rangle$ as functions of $K_S^0 K_S^0$ effective mass for $t' < 0.1$ (GeV/c^2). The solid curves are the results of the fit as explained in the text. Moments consistent with zero are not shown. The errors indicated correspond to changes of χ^2 of 1.0 for the mass-independent fit as described in the text.

equations developed in detail in Ref. 12 and given in our Table I. These equations express the moments as linear combinations of bilinear products of the amplitudes $L_{\lambda\pm}$, where $L_{\lambda\pm}$ represents the amplitude for production of a $K_S^0 K_S^0$ system with spin L and helicity λ via natural (+) or unnatural (−) parity exchange. Since all $m=2$ moments

were found to be consistent with zero, λ is restricted to the values 0 or 1. Consequently, we adopt a shorthand notation and define $L_0 = L_{0-}$ and $L_{\pm} = L_{1\pm}$. Since L must be even for a $K_S^0 K_S^0$ system, the set of production amplitudes to be considered reduces to $S_0, D_0, D_+, D_-, G_0, G_+,$ and G_- . However, the absence of any $\langle Y_8^1 \rangle$ and $\langle Y_8^2 \rangle$

moment indicates that G_+ and G_- are negligible. Furthermore, in the region of low t' , where one-pion exchange is expected to dominate, the D_+ and D_- amplitudes are small, though nonzero. To obtain good starting values for the amplitude fit described below, we initially set D_+ and D_- to zero and extracted approximate S_0 , D_0 , and G_0 amplitudes from the measured moments. The equations relating amplitudes to moments will, in general, yield multiple solutions. Having restricted ourselves to a relatively small number of amplitudes, all with $\lambda=0$, we enumerated the ambiguous solutions and examined their characteristics by a straightforward application of the Barrelet-zero technique.¹⁸ For each of the mass intervals used to determine the $\langle Y_l^m \rangle$, we then obtained several sets of complex amplitudes, each of which reproduce the observed moments. Specifically, below $M(K_S^0 K_S^0)=1.6 \text{ GeV}/c^2$, where the G_0 amplitude is negligible, there are only two solutions, characterized by the same S_0 and D_0 moduli, but differing in the sign of the S_0 - D_0 relative phase. (These solutions are in fact complex conjugates of each other.) Above $M(K_S^0 K_S^0)=1.6 \text{ GeV}/c^2$, where the G_0 amplitude is nonzero, there are four solutions, characterized by two different moduli, each with two different phases. These solutions were then used as starting values to determine a full set of amplitudes (now including the D_+ and D_- amplitudes) from the moments using the coupled equations of Table I. Each solution is represented by a set of seven parameters per mass bin, where the

parameters are the squared moduli of the S_0 , D_0 , D_+ , D_- , and G_0 amplitudes, and the phase differences $|\phi_S - \phi_D|$ and $|\phi_G - \phi_D|$. Two solutions are shown in Fig. 5, where each is understood to be one of a complex conjugate pair of solutions. The D_+ and D_- amplitudes (not shown in Fig. 5) are small. We note that these amplitudes are sums over $K_S^0 K_S^0$ isospin states as well as over target- and recoil-nucleon helicity states since none of these quantum numbers is observable in this experiment. However, since the $K_S^0 K_S^0$ system must be in an even spin state, the $I=0$ amplitudes and nucleon helicity-flip amplitudes dominate, since one-pion exchange (OPE) dominates¹⁰ at low t' . Furthermore, a recent $K^+ K^-$ experiment with a polarized target¹⁹ has demonstrated that the simple model assuming spin-flip dominance, phase coherence, and identical vanishing of $m=2$ moments, is indeed a sufficient tool for an energy-independent partial-wave analysis.

In order to determine the meson spectrum, a mass-dependent fit to the moments was performed, representing the amplitudes as a sum of complex Breit-Wigner forms plus simple smooth backgrounds. These amplitudes were fitted against the measured moments of Fig. 4 by χ^2 minimization. In general, each Breit-Wigner form has an arbitrary production phase associated with it. However, the f - and h -meson Breit-Wigner absolute production phases were chosen to be zero, consistent with the known $\pi\pi \rightarrow \pi\pi$ results for those two resonances. The Breit-Wigner amplitudes are given

TABLE I. Spherical harmonic moments in terms of t -channel helicity amplitudes L_0 , L_+ , and L_- . Terms of the form L^2 stand for $|L|^2$, and terms of the form $L_1 L_2$ stand for $\text{Re}(L_1 L_2^*)$. Summation over target- and recoil-nucleon helicity states is implied such that, for instance, $L^2 = |L|^2 = |L_{\text{flip}}|^2 + |L_{\text{nonflip}}|^2$.

$$\begin{aligned}
\sqrt{4\pi N} \langle Y_0^0 \rangle &= S_0^2 + D_0^2 + D_+^2 + D_-^2 + G_0^2 + G_+^2 + G_-^2 \\
\sqrt{4\pi N} \langle Y_2^0 \rangle &= 0.639D_0^2 + 0.319(D_-^2 + D_+^2) + 0.581G_0^2 + 0.494(G_-^2 + G_+^2) \\
&\quad + 2S_0 D_0 + 1.714D_0 G_0 + 1.565(D_- G_- + D_+ G_+) \\
\sqrt{4\pi N} \langle Y_2^1 \rangle &= 1.414S_0 D_- + 0.452D_0 D_- + 1.107D_0 G_- - 0.808D_- G_0 + 0.225G_0 G_- \\
\sqrt{4\pi N} \langle Y_2^2 \rangle &= 0.391(D_-^2 - D_+^2) + 0.356(G_-^2 - G_+^2) - 0.319(D_- G_- - D_+ G_+) \\
\sqrt{4\pi N} \langle Y_4^0 \rangle &= 0.857D_0^2 - 0.571(D_-^2 + D_+^2) + 0.486G_0^2 + 0.243(G_-^2 + G_+^2) \\
&\quad + 2S_0 G_0 + 1.162D_0 G_0 + 0.318(D_- G_- + D_+ G_+) \\
\sqrt{4\pi N} \langle Y_4^1 \rangle &= 1.414S_0 G_- + 1.107D_0 D_- + 0.698D_0 G_- + 0.225D_- G_0 + 0.343G_0 G_- \\
\sqrt{4\pi N} \langle Y_4^2 \rangle &= 0.452(D_-^2 - D_+^2) + 0.453(D_- G_- - D_+ G_+) + 0.256(G_-^2 - G_+^2) \\
\sqrt{4\pi N} \langle Y_6^0 \rangle &= 1.691D_0 G_0 - 1.235(D_- G_- + D_+ G_+) + 0.504G_0^2 - 0.025(G_-^2 + G_+^2) \\
\sqrt{4\pi N} \langle Y_6^1 \rangle &= 1.155D_0 G_- + 1.055D_- G_0 + 0.517G_0 G_- \\
\sqrt{4\pi N} \langle Y_6^2 \rangle &= 0.844(D_- G_- - D_+ G_+) + 0.258(G_-^2 - G_+^2) \\
\sqrt{4\pi N} \langle Y_8^0 \rangle &= 0.831G_0^2 - 0.665(G_-^2 + G_+^2) \\
\sqrt{4\pi N} \langle Y_8^1 \rangle &= 1.115G_0 G_- \\
\sqrt{4\pi N} \langle Y_8^2 \rangle &= 0.421(G_-^2 - G_+^2)
\end{aligned}$$

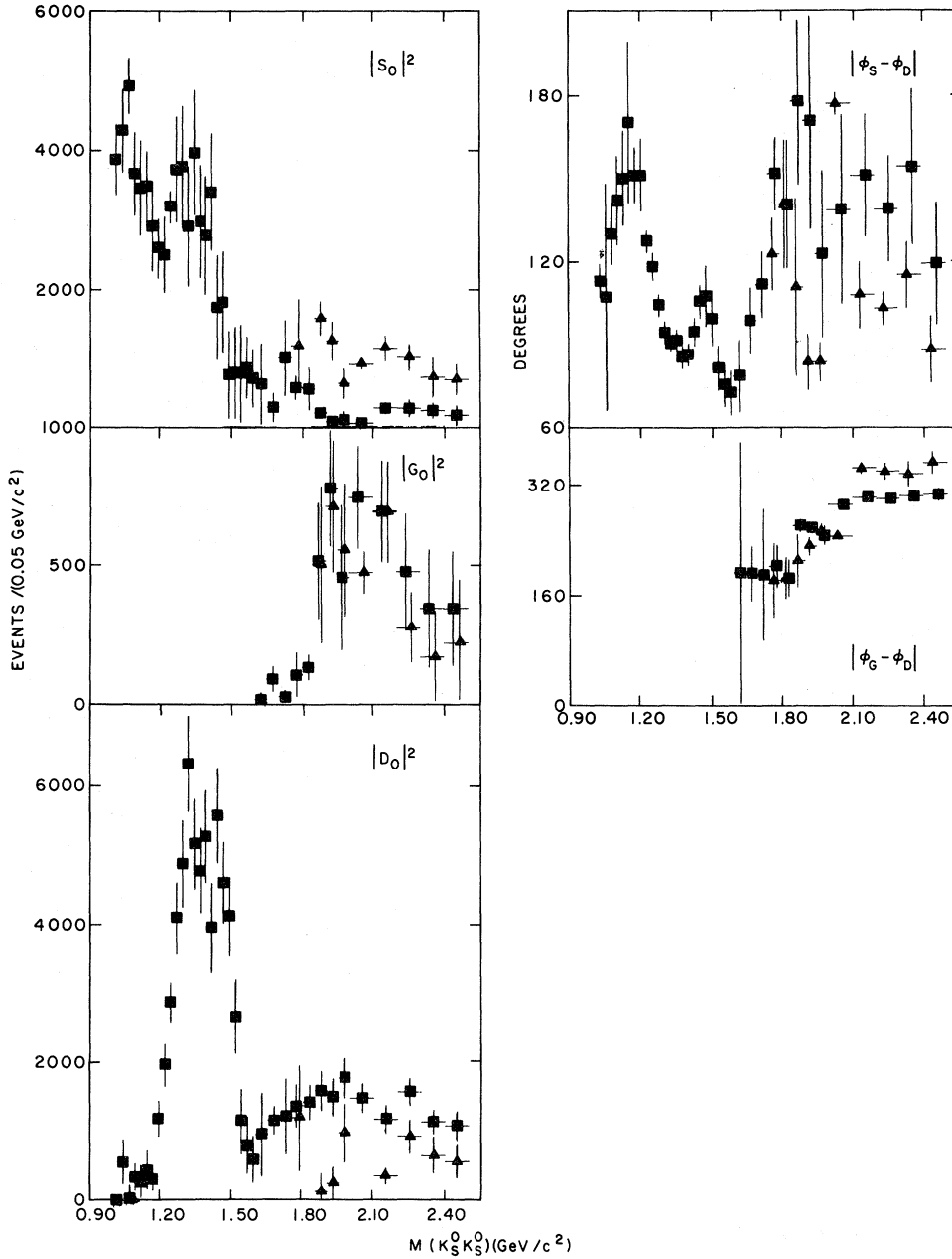


FIG. 5. The square of the moduli of the S_0 , D_0 , and G_0 amplitudes as functions of $K_S^0 K_S^0$ effective mass together with the S - D and G - D relative phases for $t' < 0.1$ $(\text{GeV}/c)^2$. Complex-conjugate ambiguities are not shown as explained in the text. The errors indicated are the result of propagating the errors on the moments.

by

$$A_l^m(s) = \frac{[q_{K\bar{K}} B_l(rq_{K\bar{K}})]^{1/2} S_R(l, m)}{m_R^2 - s - im_R \Gamma_{R, l}},$$

where l is the angular momentum, $S_R(l, m)$ is a complex number which was set positive real for

the f and h mesons, $q_{K\bar{K}}$ is the center-of-mass momentum of the $K\bar{K}$ system, and $B_l(rq_{K\bar{K}})$ is the Blatt-Weisskopf barrier factor which depends on the radius of interaction r (chosen to be 1 fm), the angular momentum l , and the center-of-mass momentum q . The center-of-mass energy squared

of the $K\bar{K}$ system is denoted by s , and m_R is the mass of the resonance. The total width of resonance R was approximated by

$$\Gamma_{R,l} = q_{ij} B_l(rq_{ij}) \gamma_R^2,$$

where i and j refer to the two particles that are the dominant decay mode of R , $B_l(rq_{ij})$ is the barrier factor for that mode, and γ_R^2 is the coupling constant of the resonance. In the case of the $S^*(980)$, it was necessary to include two terms in the total width, since the $K\bar{K}$ partial width is very important but vanishes below $K\bar{K}$ threshold. Hence both $\pi\pi$ and $K\bar{K}$ contributions were included in the total width for the S^* .

The smooth coherent backgrounds which were used for the D_0 wave and S_0 wave are as follows. For the D_0 wave, we used the same Breit-Wigner form given above with a large value for the mass and width. A third-order complex polynomial was also tried, but was not as good at representing the background as the low-energy tail of a broad, high-mass, Breit-Wigner form. For the S_0 wave, we used the background parametrization of Ref. 10, namely, a pole-free K -matrix form. We have extended it to higher masses by a fourth-order complex polynomial arranged to join the lower mass form smoothly at $1.53 \text{ GeV}/c^2$. More will be said about this background in Sec. VI.

Due to the number of fit parameters involved and the ambiguities inherent in the amplitudes, we found many acceptable mass-independent fits. They are divisible into three classes.

The first class is characterized by a very large f' amplitude. We reject solutions of this class since they are inconsistent with the known mixing angle of the f - f' system and show a large D_0 phase motion between 1.5 and $1.6 \text{ GeV}/c^2$, inconsistent with the results of Ref. 10. The second class of solutions is characterized by a large, smooth, D_0 -wave background above $1.6 \text{ GeV}/c^2$. The third class of solutions contains a narrow D_0 -wave resonance around $1.88 \text{ GeV}/c^2$.

All three classes of solution require a new S_0 wave resonance between 1.7 and $1.8 \text{ GeV}/c^2$. Acceptable fits (from the χ^2 point of view) were found in all three classes, but we prefer one solution of class two because it required the smallest number of new resonances (one). This solution gave a χ^2 of 327 for 293 degrees of freedom, and the properties of the resonances determined by this fit are given in Table II. The curves shown in Figs. 4 and 6 correspond to this solution. The points shown on Fig. 6 are those from Fig. 5 which remain after resolution of the ambiguities by our preferred solution.

The errors given in Table II are not the statisti-

TABLE II. Parameters from the mass-dependent fits as described in the text. The errors for a given parameter indicate the full range of values obtained over the set of acceptable fits rather than the statistical errors associated with any single fit. Values without errors are effectively fixed as explained in the text.

Particle	Mass (GeV/c) ²	Width (GeV/c) ²	$B d\sigma/dM$ $t' \leq 0.1 \text{ (GeV}/c)^2$ [nb/(GeV/c) ²]
<i>S</i> wave			
S^*	$0.985^{+0.009}_{-0.039}$	$0.060^{+0.141}_{-0.010}$	
ϵ	$1.463^{+0.009}_{-0.009}$	$0.118^{+0.138}_{-0.016}$	172^{+547}_{-74}
$S^{*'}$	$1.771^{+0.077}_{-0.053}$	$0.200^{+0.156}_{-0.009}$	174^{+567}_{-52}
<i>D</i> wave			
f	1.277	0.170	709^{+227}_{-369}
A_2	1.304	0.109	7^{+227}_{-7}
f'	1.525	0.090	167^{+37}_{-77}
<i>G</i> wave			
h	$2.031^{+0.025}_{-0.036}$	$0.305^{+0.036}_{-0.119}$	98^{+65}_{-23}

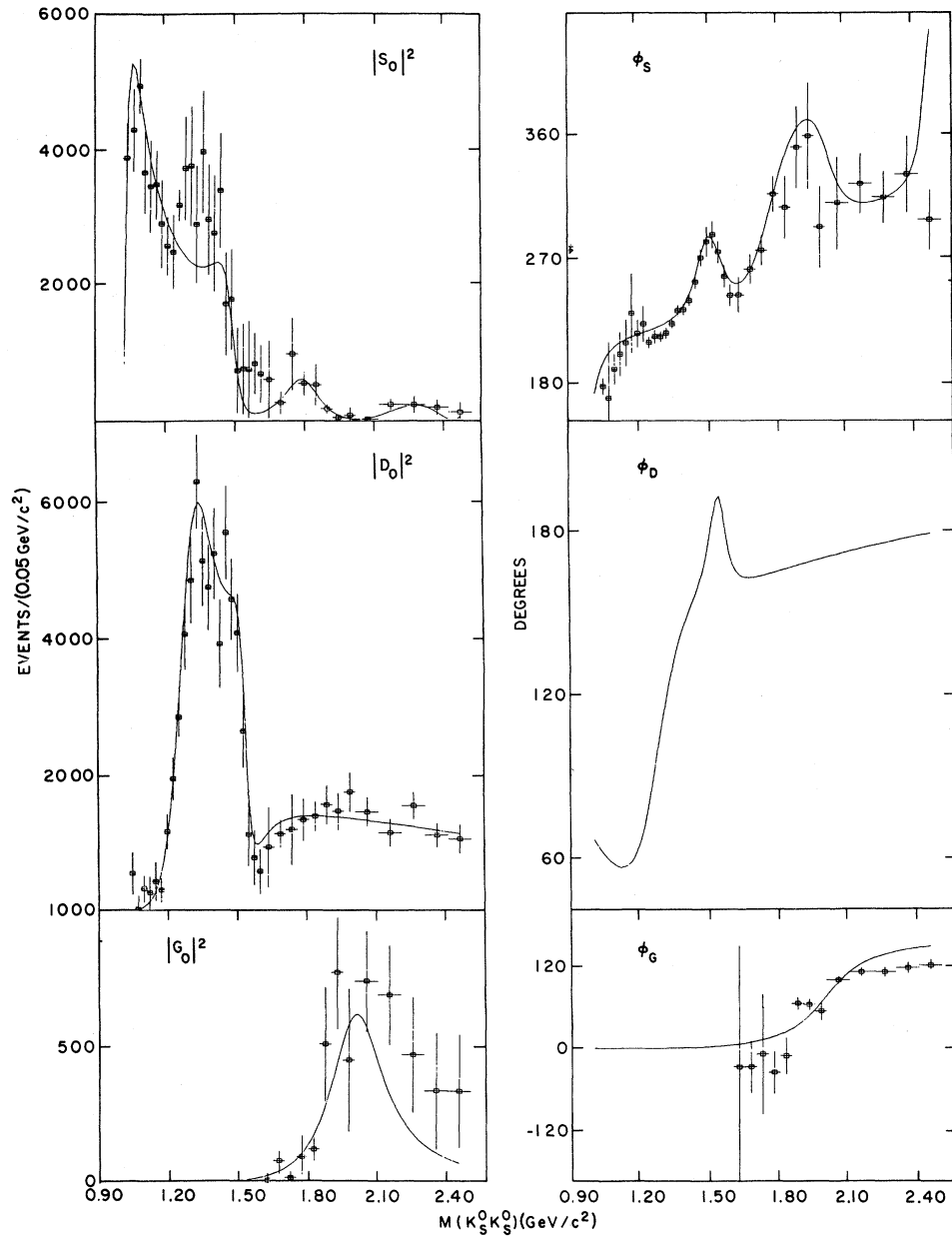


FIG. 6. The square of the moduli of the S_0 , D_0 , and G_0 amplitudes together with their absolute phases from our best fit as functions of $K_S^0 K_S^0$ effective mass for $t' < 0.1$ (GeV/c^2). The solid curves are the results of our preferred mass-dependent fit in the same t' interval.

cal errors associated with our favored solution alone. We have chosen instead to enlarge the errors to indicate the full range of values obtained from all six acceptable fits of classes 2 and 3. We emphasize that the values given in Table II are those obtained from our preferred solution alone. In the case where that solution has assigned some

parameter a value which is near the limit of the range of values defined by all six acceptable fits, the errors on that parameter appear highly asymmetric. The widths of all three S -wave states in the table are examples of this consequence of our procedure. Nevertheless, we feel this is a more reasonable estimate of the systematic uncertainty in

these parameters than the (much smaller) statistical errors associated with any single fit. Note also that no mass or width errors are given for any of the known D -wave states. Those masses and widths were allowed to vary only within narrow ranges about their accepted values and should thus be regarded as effectively fixed with no meaningful error. The column labeled $B d\sigma/dM$ in Table II is the cross section for production of the corresponding resonance, evaluated at the resonance mass for $t' < 0.1$ (GeV/c)², times the branching ratio for decay into $K_S^0 K_S^0$. The errors were obtained in the same way as those on masses and widths. A correction for unseen K_S^0 decays has been included. Expressed in this way, these cross sections are independent of the Breit-Wigner shape we have chosen. However no value is given for the $S^*(980)$ since its resonance mass lies below threshold.

The only new state in Table II we have called the $S^{**}(1770)$ since it appears to be the next S -wave resonance strongly coupled to the $K\bar{K}$ channel after the $S^*(980)$. This resonance is crucial in understanding the $\langle Y_2^0 \rangle$ moment around 1.8 GeV/c². The strong interference seen near that mass in the $\langle Y_2^0 \rangle$ moment is the most graphic evidence for the S^{**} in our data. Without the S^{**} in the fit, the predicted $\langle Y_2^0 \rangle$ moment is small and featureless for $K_S^0 K_S^0$ masses between 1.6 and 1.9 GeV/c², in violent disagreement with the data in a region where the errors are small. The inability to account for that interference and for the corresponding phase motion in the S -wave amplitude in the same mass region worsens the χ^2 by 250.

In order to understand the significance of this 250 in χ^2 , we have derived a σ test in an appendix. In the case where one has a large number of degrees of freedom, the physical significance of any single effect in terms of σ is approximately equal to the χ^2 difference divided by the square root of

twice the overall χ^2 . In our best fit, the S^{**} represents a 10σ effect.

Note that the 1.85-GeV/c² D -wave state which was a prominent feature of Ref. 14 does not appear prominently in our D -wave amplitude. We could fit our D wave above 1.6 GeV/c² with several overlapping states but with no significant χ^2 improvement over the smooth curve we have called "background." We note that four of the solutions of Ref. 14 show an enhancement in the modulus of the S -wave amplitude around 1.65 GeV/c² but no S -wave phase data are presented beyond 1.55 GeV/c².

V. RESULTS

The first, and completely model-independent, result of this experiment is the cross section for $\pi^- p \rightarrow K_S^0 K_S^0 n$ at 23 GeV/c. For $t' < 0.1$ (GeV/c)², we find $\sigma(\pi^- p \rightarrow K_S^0 K_S^0 n) = 1.04 \pm 0.14 \mu\text{b}$, including a correction for unseen K_S^0 decays. Note that a cross section for larger t' intervals can be obtained from the fact that our t' distribution has a slope of approximately -8.0 (GeV/c)⁻².

The most important single result of our amplitude analysis is the appearance of a new and previously unobserved state with $J^P = 0^+$, which we call the $S^{**}(1770)$. The relative production ratios of states in the same SU(3) multiplet are the most model-independent results that one can obtain other than the cross sections of Table II. We have summarized our results for the ratio of $f'(1515)$ to $f(1270)$ production and of $S^{**}(1770)$ to $\epsilon(1450)$ production in Table III. Just as for the cross sections, however, these production ratios are somewhat fit-dependent. The values given in the table are the averages within each fit class, whereas the errors indicate the full range over all solutions in that fit

TABLE III. Production ratios for f' and f mesons and for S^{**} and ϵ mesons by fit class (as defined in the text). The errors given indicate the full range of values obtained within a given fit class. The best-value error shows the range of values over fit classes 2 and 3.

Class	f'/f production ratio	S^{**}/ϵ production ratio
1	$2.38^{+1.43}_{-1.36}$	$0.58^{+0.18}_{-0.21}$
2	$0.20^{+0.17}_{-0.10}$	$1.02^{+0.52}_{-0.52}$
3	$0.22^{+0.08}_{-0.06}$	$2.47^{+1.09}_{-1.09}$
best value	$0.23^{+0.14}_{-0.13}$	$1.02^{+2.11}_{-0.52}$
		Mixing angle = 45^{+7}_{-6}

class as described earlier. The ratio corresponding to our best solution (as discussed in the previous section) is given separately with an error indicating the full range of acceptable values over fit classes 2 and 3.

We assume that the $S^{*'}(1770)$ is the $s\bar{s}$ member of the $q\bar{q}$, $l=1$, 0^{++} nonet. Then, using the SU(3) Clebsch-Gordan coefficients for $0^+ \rightarrow 0^- 0^-$ of Ref. 20, and assuming that the g_8 and g_0 are such that ideal mixing occurs at 35° , we can determine the ratio of ϵ and $S^{*'}$ amplitudes in our fit. Table III gives the mixing angle for our best fit. Since this mixing angle implies a substantial $\pi\pi$ decay width, one would expect to see evidence for the $S^{*'}$ state in the appropriate $\pi\pi$ amplitudes. Solution B of Corden *et al.*,²¹ while not their favored solution, does indeed show resonance behavior at $1.75 \text{ GeV}/c^2$ in the S -wave amplitude in their study of $\pi\pi$ scattering at 12 and 15 GeV/c .

Another important result from our analysis is summarized in Table IV, where we present our values for the branching ratios $(f \rightarrow K\bar{K})/(f \rightarrow \text{all})$ and $(h \rightarrow K\bar{K})/(h \rightarrow \text{all})$. Again, we have given these branching ratios separately for each solution class as well as for our best solution. The errors are obtained in the same manner as those given in Table III and, again, reflect the systematic uncertainties inherent in this kind of analysis. To determine these branching ratios, it was necessary to know the absolute scale of unitarity for the D and G waves, assuming that the f and h mesons are produced by $\pi\pi$ scattering. In both cases, this was accomplished by using the standard OPE formalism.⁹ For the f meson, using the D -wave unitarity scale, our measured cross sections of Table II and the branching ratio for $f \rightarrow \pi\pi$ from Ref. 22, we have computed the $f \rightarrow K\bar{K}$ branching ratios; these are summarized in Table IV. Likewise, the G -wave unitarity scale, together with the $h \rightarrow \pi\pi$ branching ratio of Ref. 21, leads to the $h \rightarrow K\bar{K}$

branching-ratio values summarized in Table IV. We shall defer a comparison of our best-fit value with those from other experiments until Sec. VI.

VI. COMPARISON WITH OTHER ANALYSES

We begin this section with a comparison of the t -channel moments of our data with those of earlier experiments. We have thus far restricted our attention to the t' interval $0.0 < t' < 0.1 \text{ (GeV}/c)^2$. However, the authors of both Ref. 3 and Ref. 5 have instead chosen the interval $0.0 < t' < 0.2 \text{ (GeV}/c)^2$. We have extracted acceptance-corrected moments from our data in the higher- t' region, using the procedure already described in Sec. III. For the $0.1 < t' < 0.2 \text{ (GeV}/c)^2$ data, we have chosen $K_S^0 K_S^0$ effective-mass bins of $0.05 \text{ GeV}/c^2$ for $M(K_S^0 K_S^0) < 1.6 \text{ GeV}/c^2$ and bins of $0.1 \text{ GeV}/c^2$ thereafter. This choice was made on statistical grounds, the mass resolution again being less than the bin size. These moments were then combined statistically with those from the $t' < 0.1 \text{ (GeV}/c)^2$ region, and are shown in Fig. 7 together with those from Refs. 3 and 5 for the $K_S^0 K_S^0$ effective-mass interval $M(K_S^0 K_S^0) < 1.6 \text{ GeV}/c^2$, where all three experiments had significant data. For this comparison, we have scaled the moments of Refs. 3 and 5 so as to have the same value of $\sum \langle Y_0^0 \rangle$ as in our data, summed over the $K_S^0 K_S^0$ effective-mass interval indicated. The agreement among the three experiments is quite good.

Next, we compare the results of our D -wave fit to the moments. For the D wave, we will compare our results summarized in Tables III and IV with those of other $K\bar{K}$ experiments. In the mass range below $1.6 \text{ GeV}/c^2$, it is well established that only one D -wave solution exists, dominated by the f and f' resonances. In Table V, we compare our f'/f production ratio with those from four other experi-

TABLE IV. Branching ratios for $f \rightarrow K\bar{K}$ and $h \rightarrow K\bar{K}$ decays. We define $X_K = \Gamma_{K\bar{K}}/\Gamma_T$, using $\Gamma_{\pi\pi}/\Gamma_T = 0.83$ from Ref. 22 for $f \rightarrow \pi\pi$, and $\Gamma_{\pi\pi}/\Gamma_T = 0.17$ from Ref. 21 for $h \rightarrow \pi\pi$. The errors were obtained in the same manner as those in Table III.

Class	X_K for $f \rightarrow K\bar{K}$ (%)	X_K for $h \rightarrow K\bar{K}$ (%)
1	$3.7^{+3.1}_{-1.9}$	$0.80^{+0.17}_{-0.15}$
2	$3.1^{+0.7}_{-1.7}$	$0.70^{+0.21}_{-0.18}$
3	$3.0^{+0.7}_{-0.8}$	$0.98^{+0.10}_{-0.11}$
best value	$3.1^{+0.7}_{-1.7}$	$0.67^{+0.41}_{-0.15}$

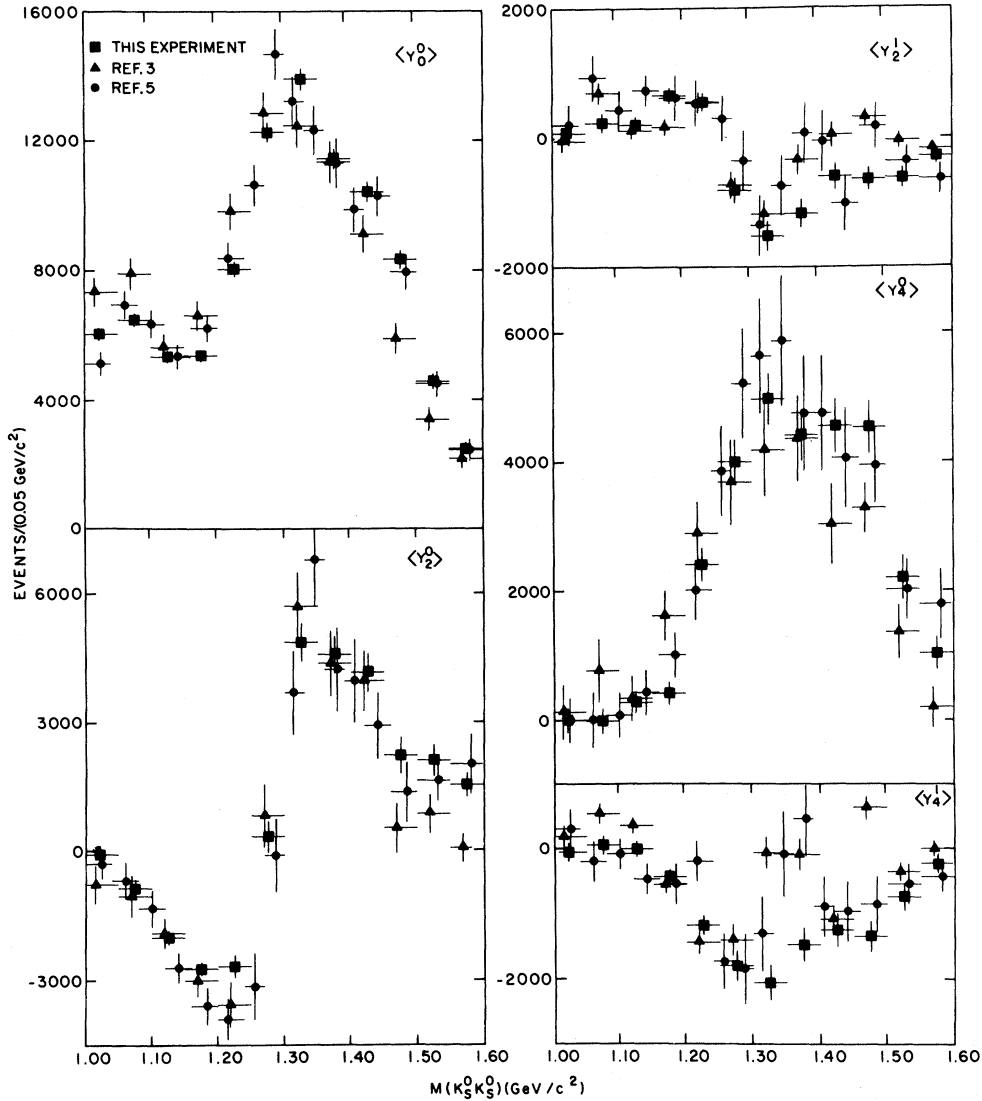


FIG. 7. Comparison of our moments as functions of $K_S^0 K_S^0$ effective mass with those of Refs. 3 and 5 for $t' < 0.2$ $(\text{GeV}/c)^2$ and $M(K_S^0 K_S^0) < 1.6 \text{ GeV}/c^2$. The moments of Refs. 3 and 5 have been scaled to our $\sum \langle Y_i^0 \rangle$ as described in the text. Note that some points have been displaced from the bin centers to avoid overlapping error bars.

TABLE V. Comparison of f'/f production ratios obtained from several analyses.

Source	f'/f production ratio
Ref. 3	0.14 ± 0.04
Ref. 9	0.30 ± 0.03
Ref. 14	0.225 ± 0.075^a
Ref. 19	$0.346^{+0.423}_{-0.077}^a$
This experiment	$0.23^{+0.14}_{-0.13}$

^aValue computed by us from data of cited reference.

ments. All experiments find quite similar results, in particular, requiring that the f meson and the f' meson be 180° out of phase relative to one another.

Table VI is our comparison of the branching ratio $(f \rightarrow K\bar{K})/(f \rightarrow \text{all})$ with the results of five other experiments. To some extent, this table is also a test of the assumption of OPE dominance on the charge-exchange $\pi\pi$ and $K\bar{K}$ amplitudes. Some of these branching ratio values, notably those from Refs. 9 and 19, represent direct measurements. Similarly, the authors of Ref. 3 have relied on an older bubble-chamber experiment to determine the

absolute cross section in the same $K\bar{K}$ mass and t range. The other experiments listed in Table VI have used an OPE model as a way of determining this branching ratio. In our case, we have verified that our OPE formalism reproduced the cross section for f -meson production of Ref. 9 at 6 GeV/ c . We have also verified that our procedure gives correct results when compared with the cross sections of Ref. 23 at 17 GeV/ c . The agreement among the results of different experiments listed in Tables V and VI demonstrates that the D wave and OPE are quite solid and well established.

With this success for the D wave, we next turn to the G wave. We have only one other experiment which reports a G -wave cross section for h into $K\bar{K}$. We can apply our OPE model to this cross section and our cross section from Table II, plus the branching ratio of 17% for $h \rightarrow \pi\pi$ from Ref. 21 to obtain a branching ratio for $h \rightarrow K\bar{K}$ of $(2.4 \pm 1.2)\%$ for Ref. 24 and $(0.67_{-0.15}^{+0.41})\%$ for ours. These two measurements have errors that differ by a factor of 3, which is surprising since the number of events obtained by the two experiments is approximately equal. We believe this factor comes from the less restrictive nature of the K^+K^- experiment. For our experiment, the $\langle Y_8^0 \rangle$ moment completely determines the amount of h meson present, whereas the K^+K^- experiment had to fit the $\langle Y_6^0 \rangle$, $\langle Y_7^0 \rangle$, $\langle Y_8^0 \rangle$, $\langle Y_9^0 \rangle$, and $\langle Y_{10}^0 \rangle$ moments with the F -wave $g(1680)$, the G -wave $h(2040)$, and an H -wave background.

We have reserved the discussion and comparison of our S -wave amplitudes with those arising from the different analyses until now. This was done because of the complications that arise in doing mass-dependent fits to the $K\bar{K}$ mass interval between threshold and 1.6 GeV/ c^2 . For the higher-mass region, the S -wave behavior is well described by the S^{*} resonance with a smooth background.

This solution arose quite naturally from the smooth and structureless nature of the D wave in the higher-mass region, which then requires that all of the S - D relative-phase motion be due to the S -wave amplitude. Along with the phase motion, a maximum in the S -wave amplitude is likewise observed at the mass where the phase motion is largest.

Before discussing these complications, we first compare the squared moduli and S - D relative phases of our analysis with those of Refs. 3, 5, 10, and 14. Figure 8(a) shows $|S_0|^2$ for all the $K_S^0 K_S^0$ experiments plotted together in the lower-mass region where comparison is meaningful. Figure 8(b) shows $|S_0|^2$ for two K^+K^- experiments plotted against our $|S_0|^2$. One can see that the five mass-independent analyses give very consistent results (for the moment, ignore the curves on the plot). On the other hand, comparison of the S - D relative phases shown in Figs. 9(a) and 9(b), shows that while we agree closely with the results from other $K_S^0 K_S^0$ experiments [Fig. 9(a)], we disagree with K^+K^- experiments, particularly in the threshold region and around the ϵ resonance at 1.43 GeV/ c^2 .

There is a simple way to interpret the S - D -wave relative-phase motion. Since it is known that several resonances are present and contribute to the S - or D -wave amplitudes, there will in general be a counterclockwise motion of the two amplitudes. The average of this counterclockwise phase motion will be undetectable since we observe only relative phases. However, at a resonance mass, we expect a net positive excursion of $\phi_S - \phi_D$ for an S -wave resonance, and a net negative motion for a D -wave resonance. Even though Figs. 9(a) and 9(b) represent two ambiguous solutions generated by choosing opposite signs for the relative phase (i.e., $\pm |\phi_S - \phi_D|$), the figure as plotted is the correct

TABLE VI. Comparison of $f \rightarrow K\bar{K}$ branching ratios obtained from several analyses.

Source	Beam momentum (GeV/ c)	$(f \rightarrow K\bar{K})/(f \rightarrow \text{all})$
Ref. 3	6.0 and 7.0	0.023 ± 0.008
Ref. 5	8.9	0.024 ± 0.005^a
Ref. 9	6.0	0.038 ± 0.004
Ref. 14	10.0	0.029 ± 0.004^a
Ref. 19	17.2 and 18.4	$0.058_{-0.026}^{+0.019}$
This experiment	23.0	$0.031_{-0.017}^{+0.007^a}$

^aValue obtained by extrapolation to pion pole.

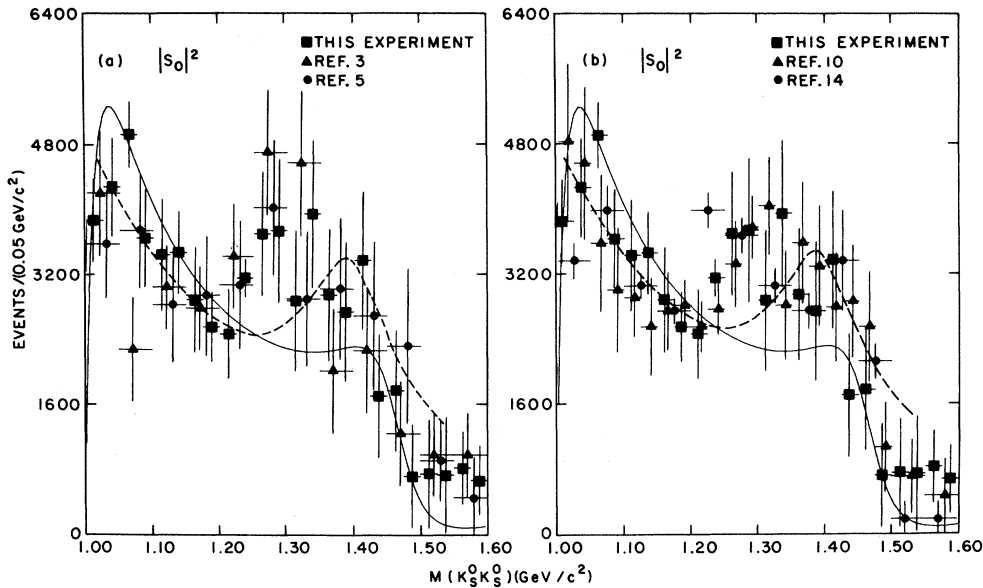


FIG. 8. Comparison of the squared modulus of our S -wave solution as a function of $K\bar{K}$ effective mass with those of Refs. 3 and 5 in (a), and with those of Refs. 10 and 14 in (b) for $M(K\bar{K}) < 1.6 \text{ GeV}/c^2$. The solid curve is the result of our mass-dependent fit. The dashed curve is the fit of Ref. 25 to the data of Refs. 10 and 23. Note that some points have been displaced from the bin centers to avoid overlapping error bars.

choice for the resolution of the ambiguity. This is clear from the backward phase motion that occurs around the $f(1270)$ -meson mass. Starting at the highest masses and continuing towards lower masses, we see backward phase motion around the $f'(1515)$ meson, and then forward phase motion around the $\epsilon(1450)$ meson. However, this forward phase motion occurs at $1.43 \text{ GeV}/c^2$ for Ref. 10, where they claim the ϵ resonance, as compared to $1.46 \text{ GeV}/c^2$ for our ϵ resonance. Continuing towards lower $K\bar{K}$ mass, we then see backward phase motion again at the $f(1270)$ mass, and, in our results as well as those of Ref. 3, forward phase motion due to the $S^*(980)$ at threshold. On the other hand, Ref. 10 shows no phase motion near threshold. We note that Ref. 10 presents results of a K^+K^- analysis, and hence had to deal with ambiguities arising from the presence of P waves.

With this as an introduction, we can now describe our mass-dependent fit to the moments of Fig. 4. Even though we achieve a good fit to the moments, we do a poor job of describing the S wave near $1.3 \text{ GeV}/c^2$ as seen from Figs. 6, 8(a), and 8(b). In general, the S wave has had a history of being difficult to parametrize. Reference 10 has found that the region from threshold to $1.6 \text{ GeV}/c^2$ is well parametrized by a pole-free K -

matrix formulation to account for the threshold behavior and the ϵ resonance. Noting that success, we have adopted their background for our threshold region. A fit using this background and the ϵ gives a fit to the $|S_0|^2$ that is very similar to our best fit as shown in Figs. 6 and 8. In addition to not agreeing with the mass-independent amplitudes in the $1.3 \text{ GeV}/c^2$ region, this parametrization does not represent the S -wave threshold phase motion well. In order to improve the threshold behavior, and possibly the $1.3\text{-GeV}/c^2$ region, we have added the well-known, though somewhat controversial, $S^*(980)$. This did improve the threshold behavior, reducing the χ^2 by 15, which by our σ test is only a 0.6σ effect. However, phase motion does occur in the $\pi\pi$ channel so, if the S^* is indeed a resonance, it should be present in our data. The parameters for the S^* are given in Table II. This addition had no effect on the fit in the $1.3\text{-GeV}/c^2$ region. Further comparison with Ref. 10 is difficult because the authors did not directly show a model fit to their S -wave amplitudes, mainly because of the semigraphical method they employed. Figure 33(b) of Ref. 10 does show the consistency of the one-resonance assumption by plotting the square root of the product of the $\pi\pi$ and $K\bar{K}$ branching ratios, denoted $(X_K X_\pi)^{1/2}$, derived

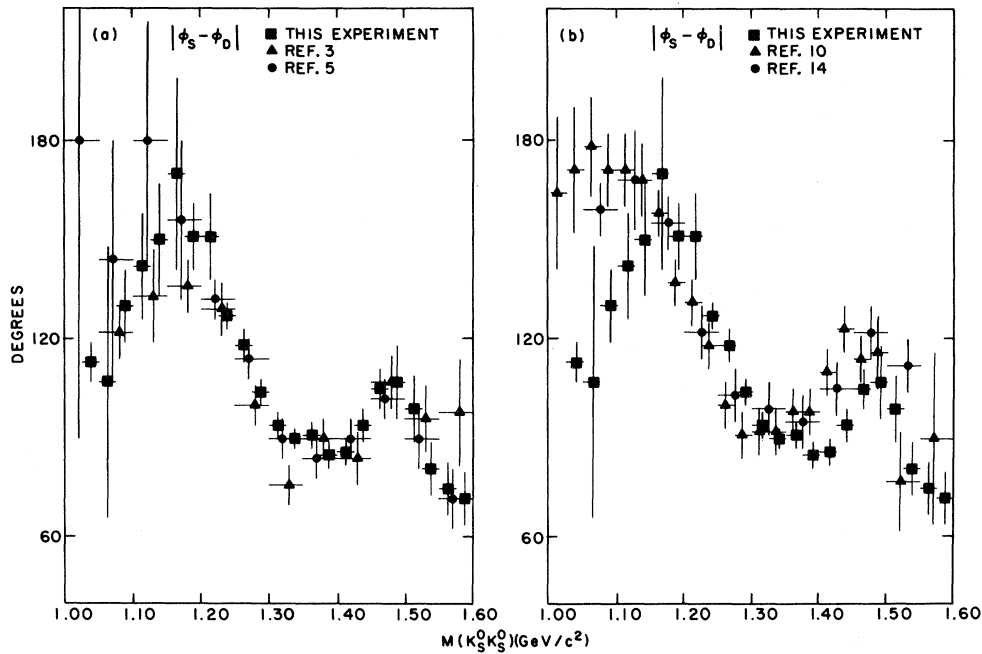


FIG. 9. Comparison of our S - D relative phase as a function of $K\bar{K}$ effective mass with those of Refs. 3 and 5 in (a), and with those of Refs. 10 and 14 in (b), for $M(K\bar{K}) < 1.6 \text{ GeV}/c^2$. Note that some points have been displaced from the bin centers to avoid overlapping error bars.

from their data. That figure shows systematic deviations in the same mass region as our Fig. 8. Finally, in a recent paper, Irving, Martin, and Done²⁵ construct a coupled-channel K -matrix fit to the $\pi\pi$ S -wave amplitudes of Ref. 23 and the $K\bar{K}$ S -wave amplitudes of Ref. 10 and obtain the fit represented by the dashed curve in Fig. 8. Their S -matrix pole parameters give an ϵ -resonance mass and width of $1.394 \text{ GeV}/c^2$ and $0.220 \text{ GeV}/c^2$, respectively. We see that their fit is also poor in the same mass region. We have likewise done fits in which we have attempted to constrain the fit to approximate the derived $|S_0|^2$ as well as the measured moments. These fits are no better than that of Ref. 25 and worsen our fit to the moments by 100 in χ^2 .

It then appears that the ϵ alone does not completely describe the ϵ -region S -wave amplitude satisfactorily. However, the physical significance of adding an extra resonance to any one analysis does not seem sufficient to claim an effect. We intend to extend our present analysis to a coupled-channel treatment using all the $\pi\pi$ and $K\bar{K}$ moments available, with the addition of a t -dependent model to separate the two isospin components in our data.

If the anomaly in the ϵ region requires an addi-

tional resonance, we will find ourselves confronted with four S -wave $I=0$ resonances of similar mass. Jaffe and Low²⁶ would assign the $S^*(980)$ to the cryptoexotic $2q2\bar{q}$ state. Two states would fit into the conventional $q\bar{q}$ model with one left over to be assigned to the ground state of the gg spectrum and thus be a glueball.

VII. SUMMARY

We have carried out a moments analysis of the $K_S^0 K_S^0$ system produced in the reaction $\pi^- p \rightarrow K_S^0 K_S^0 n$ at $23.0 \text{ GeV}/c$. From this set of moments, we have extracted the underlying amplitudes using the standard assumptions of spin-flip coherence and one-pion-exchange dominance. We derived the amplitudes from the moments by two different procedures. The first was a mass-independent procedure, using the relationships between amplitudes and moments of Table I. This procedure has a set of discrete ambiguities which can be generated by use of the Barrelet-zero method. The mass independent amplitudes are displayed in Fig. 5. Second, we parametrized the amplitudes as a sum of Breit-Wigner forms and smooth background. This mass-dependent pro-

cedure leads to three distinct classes of solutions, of which we were able to choose one as being most likely. Our best solution agrees with the known physical properties of the $\pi\pi$ and $K\bar{K}$ system observed in other experiments; all our solutions have one additional resonance in the S wave around 1.75 GeV/ c^2 . Since it is highly probable that this state has $I^G=0^+$, we call it the $S^{*'}(1770)$. If we speculate that this new resonance is the $s\bar{s}$ member of the 0^{++} $q\bar{q}$ nonet which includes the $\epsilon(1450)$ and $\kappa(1500)$, our measurement would indicate that the SU(3) singlet-octet mixing angle is 45° . Since ideal mixing occurs at 35° , one would expect to see evidence for this state in the $\pi\pi$ channel. We have also compared the $f'(1515)/f(1270)$ production ratio and the branching ratios ($f \rightarrow K\bar{K}$)/($f \rightarrow$ all) and ($h \rightarrow K\bar{K}$)/($h \rightarrow$ all) with other experiments.

Finally, we discuss the major difference between the mass-independent and mass-dependent amplitudes. This discrepancy occurs in the S wave around 1.3 GeV/ c^2 . The resolution of this discrepancy (which we call the ϵ anomaly) may indicate yet another S -wave resonance, which would be a good candidate for a glueball state. We plan to pursue this point by combining the data from other experiments with ours in a t -dependent analysis, as well as by collecting more $K_S^0 K_S^0$ data.

ACKNOWLEDGMENTS

We thank the members of the Alternating Gradient Synchrotron Division and the Experimental Planning and Support Division of the Accelerator Department of BNL for their help in the execution of this experiment. We thank the technical support staff of the MPS and OLDF for their efforts in our behalf. We likewise acknowledge the help of Dr. F. T. Dao during the early phases of the experiment and that of S. Eiseman during the data taking. We are indebted to Dr. W. Beusch for supplying us with some numerical results from Ref. 5 for comparison with our own. Special thanks are due to Dr. A. B. Wicklund for several detailed and valuable communications. We acknowledge financial support from the U. S. Department of Energy under Contracts Nos. DE-AC02-80ER10663 (Arizona), DE-AC02-76CH00016 (BNL), and DOE-ER-03023-25 (Tufts), from the National Science Foundation under Grants Nos. NSF-PHY80-09788 (CCNY) and NSF-PHY80-01621 (Vanderbilt), and from the City University of New York PSC-BHE Research Awards Program (CCNY).

APPENDIX

In this appendix, we derive the σ test referred to in the main text. We use the equation for the χ^2 distribution in the limit of the number of degrees of freedom, N_D , being large from p. S36 of Ref. 22. In this limit, the χ^2 is normally distributed about N_D with standard deviation σ of 1. Therefore the confidence level (C.L.) is approximately equal to

$$\text{C.L.} = \frac{1}{\sqrt{2\pi}} \int_y^\infty \exp(-z^2/2) dz, \quad (\text{A1})$$

where

$$y = (2\chi^2)^{1/2} - (2N_D - 1)^{1/2}. \quad (\text{A2})$$

Since the standard deviation of Eq. (A1) is 1, the difference in y for different hypotheses becomes the basis of the σ test. In other words, the number of σ 's by which two hypotheses differ is given by

$$n_\sigma = y_2 - y_1, \quad (\text{A3})$$

where

$$y_k = (2\chi_k^2)^{1/2} - (2N_{D_k} - 1)^{1/2}. \quad (\text{A4})$$

Let χ_1^2 and N_{D_1} be the χ^2 and number of degrees of freedom for the best fit with the ratio of approximately 1. We define

$$\chi_2^2 = \chi_1^2 + \Delta\chi^2 \quad (\text{A5})$$

and

$$N_{D_2} = N_{D_1} + n, \quad (\text{A6})$$

where $\Delta\chi^2$ is small compared to χ_1^2 and n is small compared to N_{D_1} . Substituting Eqs. (A5) and (A6) into (A4), we then obtain

$$n_\sigma = (2\chi_1^2 + 2\Delta\chi^2)^{1/2} - (2N_{D_1} + 2n - 1)^{1/2} - (2\chi_1^2)^{1/2} + (2N_{D_1} - 1)^{1/2}. \quad (\text{A7})$$

With the assumptions of $\Delta\chi^2/\chi_1^2$ and n/N_{D_1} being small and $\chi_1^2 \approx N_{D_1} \gg 1$, we can rewrite (A7) as

$$n_\sigma = (2\chi_1^2)^{1/2} [\Delta\chi^2/2\chi_1^2 - n/(2N_{D_1} - 1)]. \quad (\text{A8})$$

Since the last term is small, n_σ becomes

$$n_\sigma = \Delta\chi^2 / (2\chi_1^2)^{1/2}. \quad (\text{A9})$$

- *Present address: National Laboratory for High Energy Physics, KEK, Tsukuba, 305 Japan.
- †Now at City College of New York, New York, New York 10031.
- ‡Now at Laboratoire de l'Accelérateur Lineaire, F-91405 Orsay, France.
- ¹N. M. Cason *et al.*, Phys. Rev. Lett. **36**, 1485 (1976).
- ²N. M. Cason *et al.*, Phys. Rev. Lett. **41**, 271 (1978).
- ³V. A. Polychronakos *et al.*, Phys. Rev. D **19**, 1317 (1979).
- ⁴W. Beusch *et al.*, Phys. Lett. **60B**, 101 (1975).
- ⁵W. Wetzel *et al.*, Nucl. Phys. **B115**, 208 (1976).
- ⁶S. R. Gottesman *et al.*, Phys. Rev. D **22**, 1503 (1980).
- ⁷P. F. Loverre *et al.*, Z. Phys. C **6**, 187 (1980).
- ⁸A. J. Pawlicki *et al.*, Phys. Rev. Lett. **37**, 166 (1976).
- ⁹A. J. Pawlicki *et al.*, Phys. Rev. D **15**, 3196 (1977).
- ¹⁰D. Cohen *et al.*, Phys. Rev. D **22**, 2595 (1980).
- ¹¹A. D. Martin *et al.*, Phys. Lett. **74B**, 417 (1978).
- ¹²A. D. Martin *et al.*, Nucl. Phys. **B140**, 158 (1978).
- ¹³C. Evangelista *et al.*, Nucl. Phys. **B154**, 381 (1979).
- ¹⁴G. Costa *et al.*, Nucl. Phys. **B175**, 402 (1980).
- ¹⁵E. D. Platner *et al.*, in *Proceedings of the International Conference on Instrumentation for High Energy Physics, Frascati, Italy, 1973*, edited by S. Stipcich (Laboratori Nazionali del Comitato Nazionale per l'Energia Nucleare, Servizio Documentazione, Frascati, Italy, 1973), p. 673.
- ¹⁶S. J. Lindebaum, in *Proceedings of the Fourth International Symposium on NN Interactions, Syracuse, New York, 1975*, edited by T. E. Kalogeropoulos and K. C. Wali (Syracuse University, Syracuse, New York, 1975), Vol. 2, p. VII-19.
- ¹⁷F. James and M. Roos, Comput. Phys. Commun. **10**, 343 (1975).
- ¹⁸E. Barrelet, Nuovo Cimento **8A**, 331 (1972).
- ¹⁹L. Görlich *et al.*, Nucl. Phys. **B174**, 16 (1980).
- ²⁰D. Morgan, Phys. Lett. **51B**, 71 (1974).
- ²¹M. J. Cordon *et al.*, Nucl. Phys. **B157**, 250 (1979).
- ²²Particle Data Group, Rev. Mod. Phys. **52**, S1 (1980).
- ²³G. Grayer *et al.*, Nucl. Phys. **B75**, 189 (1974).
- ²⁴W. Blum *et al.*, Phys. Lett. **57B**, 403 (1975).
- ²⁵A. C. Irving, A. D. Martin, and P. J. Done, Z. Phys. C **10**, 45 (1981).
- ²⁶R. L. Jaffe and F. E. Low, Phys. Rev. D **19**, 2105 (1979).